This article has been published in International Endodontic Journal 2017 Dec; 50 Suppl 2:e109-e119.

Title: A zinc oxide-modified hydroxiapatite-based cement facilitated new crystalline-stoichiometric and amorphous apatites precipitation on dentine.

Running title: ZnO bioactivity of HAp-cements

Authors: Manuel Toledano[1*], Mayra C. Pérez-Álvarez[2], Fátima S. Aguilera[1], Estrella Osorio[1], Inmaculada Cabello[1], Manuel Toledano-Osorio[1], Raquel Osorio[1].

Institution: [1]University of Granada, Faculty of Dentistry, Dental Materials Section.
Colegio Máximo de Cartuja s/n
18071 – Granada - Spain.

[2] University of La Havana, Biomaterials Department.
San Lázaro y L. Municipio Plaza de la Revolución
La Havana- Cuba.

*Corresponding author: Prof. Manuel Toledano
University of Granada, Faculty of Dentistry
Dental Materials Section
Colegio Máximo de Cartuja s/n
18071 – Granada - Spain.
Tel.: +34-958243788
Fax: +34-958240809
Email: toledano@ugr.es

Abstract

Aim: To evaluate the remineralization ability of two dentin canal sealer cements. **Methodology:** Dentin surfaces were subjected to: i) 37% phosphoric acid (PA) or ii) 0.5 M ethylenediaminetetraacetic acid (EDTA) conditioning prior to the application of two experimental hydroxyapatite-based cements, containing sodium hydroxide (calcypatite) or zinc oxide (oxipatite), respectively. Samples were stored in simulated body fluid during 24 h or 21 d. Remineralization of the dentin surfaces were studied by Raman spectroscopy, mapping with K-means cluster and hierarchical cluster analysis were done. Nano-roughness and collagen fibrils width measurements were performed by means of an atomic force microscopy. **Results:** PA+oxipatite promoted both the highest dentin mineralization and crystallographic maturity at the dentin surface. Non-crystalline amorphous-like apatites were also formed. Dentin treated with PA+calcypatite attained the roughest surface with minimal fibril width. Crosslinking of collagen only raised in the group PA+oxipatite, after 21 d. The maximum relative mineral concentration and structure of collagen referred to amide I and ratio amide III/AGEs was achieved after using PA+calcypatite at 21 d time point. EDTA produced a lower stoichiometric hydroxyapatite with decreased maturity, at the expense of the carbonate band widening, though it favored the nucleation of carbonated calcium phosphate. **Conclusions:** Surfaces treated with PA+oxipatite attained the highest dentin remineralization with both crystalline-stoichiometric and amorphous apatites, at long term. EDTA conditioning facilitated amorphous-bulk mineral precipitation. This amorphization, more intense after using oxipatite, provided an ion-rich environment favoring *in situ* dentin remineralization.

Key words: Crystallinity, dentin, hydroxyapatite, Raman, remineralization, zinc.

Introduction

New biomaterials for use in endodontics including root-end filling, root-perforation repair or regeneration should inhibit collagen degradation at the dentine interface and facilitate dentine remineralization (Gandolfi *et al.* 2010, Osorio *et al.* 2015). Intracanal medicaments containing calcium hydroxide [$Ca(OH)_2$] are employed in regenerative endodontics (Kitikuson & Srisuwan, 2016), but they produce root fracture. Therefore, more effective alternatives to calcium hydroxide are required (Carvalho *et al.* 2016). Hydroxyapatite (HAp) based materials have been considered as potential candidates in the repair, regeneration and substitution of hard tissues (Al-Sanabani *et al.* 2013). The degree of mineralization and reparative dentine formation obtained with HAp-based materials was quicker and thicker than that produced by calcium hydroxide (Jean *et al.* 1988). Therefore, calcium hydroxide powder in association with HAp, has been proposed for this use. HAp possesses low mechanical strength and fracture toughness, which is an obstacle for its application in load-bearing areas. Thus, the enhancement of the mechanical properties of HAp would extend its scope of application (Al-Sanabani *et al.* 2013).

Zn-substituted HAp has been shown to possess enhanced bioactivity. Owing to the smaller ionic sizes of Zn^{2+}, its substitution for Ca^{2+} brings about considerable inward atomic relaxation of the surrounding oxygen ions, resulting in smaller coordination numbers with oxygen, as compared with that of Ca^{2+} in HAp (Matsunaga, 2008). This effect makes zinc attractive for use as therapeutic agent in the fields of hard tissue regeneration. The aim of this study is to compare two experimental HAp-based cements: (1) calcypatite (composed by modified HAp particles and a calcium hydroxide-based paste), and (2) oxipatite (a combination of the HAp particles, and zinc oxide).

For root canal treatment of teeth with necrotic pulp, not only foraminal but intracanal space cleanliness are necessary. The irrigation procedure may be undertaken with phosphoric acid (PA) or EDTA (ethylenediaminetetraacetic acid), but this conditioning step may damage the structural integrity of the dentine collagen, especially after using PA (Osorio *et al.* 2015). Dentine is an organic matrix that comprises about 30% type I collagen fibrils and noncollagenous proteins, such as dentine matrix proteins and dentine phosphoproteins (Xu *et al.* 2011). Noncollagenous proteins play a critical role to orchestrate dentine remineralization. They possess carboxylic and phosphate functional groups that act

as sites for calcium and phosphate nucleation (Liu *et al.* 2011). EDTA does not completely remove non-collagenous proteins from dentine, so phosphoproteins are present (Termine *et al.* 1980). It is well known that stabilized non-collagenous phosphoproteins are involved in biomineralization procedures due to their high affinity to Ca^{2+} (Li *et al.* 2012).

Detailed data about nanostructure and chemical analysis are essential to understand changes in dentine. Raman spectroscopy is an analytical technique able to measure the molecular composition by providing a spectrum that contains information regarding all the chemical bonds present within the sample (Kunstar *et al.* 2012) for investigating molecular species of both organic and inorganic components of teeth. Micro-Raman mapping technique has been a powerful method to directly analyze the dentine interface and the mineral content, and distribution, after placing the restorative material (Toledano *et al.* 2015). Single point Raman spectra, permits to image a line profile thorough a series of point-to-point sampling.. This technique is sufficiently sensitive to differences in mineral and organic compositions that can be used to identify damaged, damage-susceptible or restored areas, and possibly explain why certain regions of dentine are subject to decay. By identifying and imaging the Raman spectral features characteristics of dentinal regions, the structural differences associated with demineralized dentine (Timlin *et al.* 2000) and further remineralization can be assessed. Combining the two approaches takes advantage of their synergies for characterizing lesions and for providing objective biochemical information.

The combination of biochemical data with atomic force microscopy (AFM) techniques appears to be a valuable tool to be applied in dentine remineralization studies. Therefore, changes in the surface morphology of dentine would affect the chemo-mechanical properties (Wang *et al.* 2017), which could be reflected by the general performance of the dentine substrate. A tribological and biochemical evaluation of changes in dentine substrate is essential to gain a better understanding of these new biomaterials, as root canal sealers and remineralizing agents. The aim of this study was to investigate the chemical and tribological changes occurring after treating the dentine surface with two different cleaner-conditioners (PA *vs* EDTA), and the application of two canal sealers (calcypatite *vs* oxypatite) at two time points (24 h *vs* 21 d). The null hypothesis that was established is that no changes in chemical and tribological properties were produced at dentine surfaces after sealer cements application.

Material and methods

Specimen preparation and cement application

Twenty four human third molars, extracted for surgical reasons, without caries lesions were obtained with informed consent from donors (20–40 year of age), under a protocol approved by the Institution Review Board of the University of Granada (891/2014). The teeth were randomly selected and stored at 4ºC in 0.5% chloramine T bacteriostatic/bacteriocidal solution for up to 1 month. This storage medium was replaced weekly. A flat mid-coronal dentine disc obtained from one surface (Diagram 1 SI), one per tooth, was exposed using a hard tissue microtome (Accutom-50; Struers, Copenhagen, Denmark) equipped with a slow-speed, water-cooled diamond wafering saw (330-CA RS-70300, Struers, Copenhagen, Denmark). A 180-grit silicon carbide (SiC) abrasive paper mounted on a water-cooled polishing machine (LaboPol-4, Struers, Copenhagen, Denmark) was used to produce a clinically relevant smear layer (Koibuchi *et al.* 2001). A 37% phosphoric acid gel was applied on the exposed dentine surfaces for 15 s, and copiously water rinsed for 30 s, in half of the specimens (n=12). On the other half (n=12), EDTA-treated dentine, 0.5 M was applied for 60 s, and copiously rinsed with water for 30 s.

Two experimental hydroxyapatite-based cements were used: 1) Calcypatite composed by modified hydroxyapatite particles and a calcium hydroxide-based paste and 2) Oxipatite which is a combination of the hydroxyapatite particles and zinc oxide (ZnO). A detailed description of the chemicals and cements is provided in Table 1.

The specimens were randomly divided into the following groups (n=6) based on the tested hydroxyapatite-based cements (calcypatite *vs* oxipatite) and dentine-etching procedure [phosphoric acid (PA) *vs* EDTA]: (i) EDTA+calcypatite; (ii) PA+calcypatite; (iii) EDTA+oxipatite; (iv) PA+oxipatite. Half of the teeth in each group (n=3) were stored for 24 h in simulated body fluid solution (SBFS) (Sigma Aldrich, St Louis, MO, USA; Panreac Química SA, Barcelona, Spain) (Table 1), and the other half (n=3) for 21 d.

AFM imaging, nanoroughness and fibril diameter measurements

Dentine surfaces were polished with SiC abrasive papers up to 4,000-grit with a final polishing

procedure performed with diamond pastes (Buehler-MetaDi, Buehler Ltd.), through 1 μm down to 0.25 μm. The surfaces of the dentine disks were scanned using a tapping mode /atomic force microscopy (TM/AFM) (Nanoscope V, Digital Instruments, Veeco Metrology Group, Santa Barbara, CA, USA). The tapping mode was performed using a 1–10 Ohm-Cm phosphorus (n) doped Si tip. Changes in vertical position provide the height of the images, registered as bright and dark regions. The tip sample was maintained stable through a constant oscillation amplitude. A data scale of 1,504 μm and a slow scan rate (0.1 Hz) were employed. Three 15x15 μm and three 2x2 μm high and phase images were recorded from each surface at different positions. For each 15x15 μm image, five randomized (3x3 μm) were created to examine the intertubular (ID) and peritubular (PD) roughness of dentine. Nanoroughness (SRa, in nanometer) was measured using proprietary software (Nanoscope Software version V7). For each group, 9 roughness values were included in the analysis, corresponding to the mean roughness value of each 15x15 μm image. Collagen fibril diameter was determined from the 2x2 μm images by section analysis using data that had been modified only by plane fitting. Five fibrils were analyzed from each image. Measurements were corrected for tip broadening (Habelitz *et al*. 2002) by the equation e=2r, where e is the error in the horizontal dimension and r is the tip's radius (Takeyasu *et al*. 1996). For each group, 9 fibril diameter values were included in the analysis, corresponding to the mean fibril diameter attained at each 2x2 μm image.

As the normality assumption of the data was valid, numerical data were analyzed with Two-way ANOVA, considering dentine treatment and storage time as influencing factors for the dependent variables surface roughness and fibril width. Intertubular and peritubular roughness were analyzed separately. Student-Newman-Keuls was employed for multiple comparison tests, with statistical significance preset at $\alpha=0.05$.

Raman spectroscopy and cluster analysis

The same dentine surfaces were, then, submitted to Raman analysis using a dispersive Raman spectrometer/microscope (Horiba Scientific Xplora, Villeneuve d´Ascq, France) A 785-nm diode laser through a X100/0.90 NA air objective was employed. The Raman signal was acquired using a 600-

lines/mm grafting centered between 400 and 1,700 cm^{-1}. Chemical mapping of the surfaces were performed. For each specimen two 12μm x 12μm areas of the surfaces at different sites were mapped, using 0.5 μm spacing on the X and 0.5 on the Y axis. The output from a clustering algorithm was basically a statistical description of the cluster centroids with the number of components in each cluster. Thus, chemical mapping was submitted to K-means cluster (KMC) analysis using the multivariate analysis tool (ISys® Horiba), which includes statistical patterns to derive the independent clusters. The K-means clustering is a method of analysis based on a centroid model which aims to partition n observations into k clusters in which each observation belongs to the cluster with the nearest mean (Almahdy *et al.* 2012). The natural groups of components (or data) based on some similarity and the centroids of a group of data sets were found by the clustering algorithm once calculated by the software and the Hierarchical Cluster Analysis (HCA). To determine cluster membership, this algorithm evaluated the distance between a point and the cluster centroids. The biochemical content of each cluster was analyzed using the average cluster spectra. The observed spectra were described at 400-1700 cm^{-1} with 10 complete overlapping Gaussian lines, suggesting homogeneous data for further calculations (Ager *et al.* 2005).

As the cluster centroids are essentially means of the cluster score for the elements of cluster, the mineral and organic components of the dentine surface were examined for each cluster. A comparison of the spectra that were collected from the specimens which compose each subgroup might indicated complete overlap, suggesting similarity between both measurements. It was hence used for identifying significant spectral differences among distinct substrata. A total of 625 points were performed per map. The number of clusters, three, were chosen according to several issues, such as the dendrogram structure, the false-color maps and the cluster centroid (Bonifacio *et al.* 2010). Each cluster was assigned to a different color, thus obtaining a false color-image of the substrate on the basis of similar spectral features. Clusters were created following Ward's technique and the dendrogram was calculated applying four factor spectra or principal components, corresponding with three different components at the dentine surface (red, blue and green). For each point of analysis, all spectra described for each cluster were averaged to obtain the mean cluster spectrum. At this point, the mineral (relative presence of minerals and crystallinity) and the organic components (normalization, crosslinking, nature and

secondary structure of collagen) of dentine was assessed as in Timlin *et al*. (2000), Kunstar *et al.* (2012) and Toledano *et al*. (2016).

Results

AFM imaging, nanoroughness and fibril diameter measurements

After two-way ANOVA it was observed that dentine surface roughness (SRa) was influenced by dentine treatment ($F=60.27$; $P<0.001$ and $F=5.19$; $P=0.03$ for intertubular and peritubular dentine respectively) and by storage time ($F=52.57$; $P<0.001$ and $F=4.45$; $p=0.04$ for intertubular and peritubular dentine respectively); interactions between both variables were also significant ($F=60.86$; $P<0.001$ and $F=65.21$; $P<0.001$ for intertubular and peritubular dentine respectively). Model reliability for intertubular dentine roughness was 0.83 and 0.57 for peritubular dentine SRa.

Fibrils width was affected by dentine treatment ($F=144.13$; $P<0.001$) and storage time ($F=505.42$; $P<0.001$), interactions between variables were also significant ($F=155.79$; $P<0.001$). Model reliability was 0.95. The dentine surfaces treated with PA+calcypatite, and analyzed for intertubular dentine (ID) at 21 d attained the highest nanoroughness (SRa) among groups [90.32 (32.45) SRa] (Fig 2a). This roughest surface complies with large extended mineral-depleted zones intermingled with localized areas of strong mineralization (Fig 1e). The lowest SRa values were achieved after treating the peritubular dentine (PD) with EDTA+oxipatite, at 24 h time point [3.33 (0.52) SRa]. Nevertheless, AFM maps at 2 x 2 μm scan zone permitted to observe an undulated topography of the dentine surface made of mineral. Dentine surfaces treated with oxipatite showed an evident remineralized dentine substrate at both peritubular and intertubular locations. Nevertheless, at 2 x 2 μm scan area, strongly remineralized collagen fibrils were observed (Fig 1h). At peritubular dentine (PD) and 24 h of study, dentine surfaces treated with PA+oxipatite attained the highest SRa values.

Significant differences were not obtained when the width of the collagen fibrils were measured, among groups, at 24 h time point. However, at 21 d dentine surfaces treated with both EDTA+calcypatite, and PA+oxipatite showed the highest collagen fibril diameter [299.1 nm (50.06) and 264.96 nm (14.04) are mean and standard deviations, respectively], among groups.

Raman spectroscopy and cluster analysis

Dentine surfaces treated with EDTA or PA+calcypatite promoted an increase of mineralization at the dentine surface. The phosphate peak, area and both mineral to matrix ratio (MMR_p) and relative mineral concentration (RMC_p) at 961 cm^{-1} increased, at 24 h time point. After 21 d of study, mineralization decreased when EDTA was used as conditioning, except when RMC_p was measured, that increased ~1.7 fold. On the contrary, mineralization augmented in all cases when PA was employed. At 21 d time point, samples treated with PA+oxipatite attained the highest intensity of the phosphate peak (45.64) among groups. The intensity of the carbonate peak at 1070 cm^{-1} increased at both groups of dentine treated with PA+calcypatite and PA+oxipatite when the Raman analysis was performed at 24 h and 21 d. In general, RMC_c raised, except in the group in which dentine was treated with PA+oxipatite, measured after 21 d which decreased.

The carbonated calcium phosphate ν_2 (430, 451 cm^{-1}) increased, in general terms, when EDTA was used as conditioning with both calcypatite and oxipatite, at 24 h and 21 d time points. The use of PA as conditioning, promoted a constant increase of carbonated calcium phosphate, regardless of the type of biomaterial applied on dentine. Nevertheless, the highest intensity peak obtained after 21 d time point was achieved by PA+oxipatite (Table 2).

The full width at half maximum ($FWHM_p$) of the phosphate (PO_4^{3-}) band at 961 cm^{-1} did not change when EDTA was used to pre-treat the dentine, regardless of the type of biomaterial. PA pretreatment provoked a discrete $FWHM_p$ decrease, *i.e*, a crystallinity increase (Table 2). This crystallinity increase complied with an augmentation of the stoichiometric HAp when PA or EDTA were used, independent of the cement that was used (Table 2). Dentine treated with PA+oxipatite produced the highest band at ν_1 (963 cm^{-1}), stoichiometric HAp (Table 2). $FWHM_c$ of the carbonate (CO_3^{2-}) band at 1070 cm^{-1} augmented when EDTA pretreated the dentine, and as a consequence, crystallinity decreased. On the other hand, $FWHM_c$ diminished in general after conditioning with PA, and as result, crystallinity augmented (Table 2).

Dentine treated with PA+oxiapatite gave rise to an increase of crosslinking of collagen when both pyridinium and AGEs-pentosidine were measured after 21 d (Table 2). The intensity of the peak

related to nature of collagen at CH_2 (1450 cm^{-1}) increased at 24 h time point, but decreased after 21 d of the study when EDTA was used before both materials were applied biomaterials (Table 2).

The nature and secondary structure of collagen referred to the ratio A-I/A-III decreased when EDTA was used and increased after using PA as conditioning agent, regardless of the applied biomaterial. The highest augmentation (~ 3.78 fold) occurred when dentine was treated with PA+ calcypatite at 24 h time point. Proteoglycans, indicated at 1062 cm^{-1}, increased in dentine samples treated with PA+oxipatite group at 21 d that increased ~ 1.23 fold (Table 2). The molecular orientation (1340 cm^{-1} peak) improved when EDTA + calcypatite was employed and specimens tested at 21 d, and when PA+calcypatite was applied and dentine analyzed at any time point (Table 2).

Discussion

The presence of zinc oxide in the chemical formulation of the endodontic sealer assures new crystalline HAp formation with improved clinical performance and non-crystalline amorphous-like apatite species are encountered. This HAp ~~that~~ provides phisiopathological dentine repair due to their short degradation times. Dentine surfaces treated with both EDTA+calcypatite and PA+oxipatite showed the highest bandwidth of collagen fibrils after 21 d of study (Fig 2b). The growing of fibrils width and dentine remineralization are commonly associated (Bertassoni *et al.* 2010). Using the software analysis, reconstituted fibrils from that assessed at 24 h time point appeared to be well formed with clear D periodic banding patterns (Figs 1b, 1h). After 21 d of study, peritubular dentine treated with PA+oxipatite showed the lowest nano-roughness values among groups (EDTA+oxipatite, PA+oxipatite). Similar trend was observed at intertubular dentine, but without significant differences between them (Fig 2a). A decrease in roughness may be associated to a role of mineral maturation and it is a sight of intrafibrillar remineralization (Zurick et al, 2013).

This mineralization increase was assessed in dentine samples treated with PA+oxipatite and compared with the control group, which attained the highest values of both phosphate peak and area, among the different groups, after 21 d of storage time (Table 2). The corresponding HCA Raman images (clusters) (Fig 3d) and results (centroids) (Fig 3e), and thus the attained Raman intensities (Fig 3b) showed a generalized increase of the phosphate peak, thus denoting greater presence of this mineral. At

high phosphate concentration, calcium pyrophosphate, calcium phosphate and unstable and non-crystalline amorphous complexes are formed (Cheng & Pritzker, 1983) around the collagen fibrils. At both v_1 954 and 963 cm^{-1} Raman intensities, dentine treated with PA+oxipatite attained the highest peak values at 21 d storage time (Table 2). These values became associated to the highest mineralization of the dentine matrix (Kunstar *et al.* 2012), at the expense of stoichiometric HAp (Timlin *et al.* 2000) (Figs 1f, 1h, 3e). The presence of Zn^{2+} in oxipatite performs as Ca/P growth inhibitors (Hoppe *et al.* 2011), indicating destabilization of the amorphous state (Barrère *et al.* 2001), favoring crystallinity at the new nucleated minerals and intrafibrillar mineralization of collagen (Toledano *et al.* 2015). At 963 cm^{-1}, the stoichiometric HAp also augmented in all cases, but the lowest rise was observed when EDTA was used as conditioning, independently of the type of biomaterial (Table 2). Therefore, EDTA promoted a lower stoichiometric HAp, slowing down the active dentine remodeling, with decreased maturity (Timlin *et al.* 2000) (Fig 1g).

In addition, the increase of mineralization in dentine samples treated with PA+oxipatite, at the expenses of a rise of additional substituted or amorphous-like apatite species (Timlin *et al.* 2000), complied with an augmentation of the asymmetric peak at 956 cm^{-1}, ~1.38 fold respect to the control group (Table 2) (Fig 3e). This remineralization event is a dynamic process in which amorphous phase formation, phase stabilization, and transition of calcium phosphate continuously occur (Tramini *et al.* 2000). Generally, the HAp with poor crystallinity has the best bioactivity, biocomopatibility and biodegradability if compared with the stoichiometric HAp. This finding concurred with a decrease of $FWHM_p$, *i.e.,* higher crystallinity (0.2%) (Table 2).

The presence of a prominent carbonate band around 1070 cm^{-1} after using PA+oxipatite (Table 2) (Fig 3e) is significant because it shows the degree of carbonate substitution in the lattice structure of apatite (Salehi *et al.* 2013), meaning an increase of carbonated apatite (Lee *et al.* 2002). The formula for stoichiometric HAp is $Ca_{10}(PO_4)_6(OH)_2$. However, biological apatite is calcium deficient and contains substantial amounts of carbonate (Fulmer & Brown, 1993). Carbonated apatite is a precursor of HAp, but when it is precipitated in the presence of zinc an exchange between Zn^{2+} and Ca^{2+} occurs *in vitro* forming a substituted apatite compound (Mayer *et al.* 1994). Therefore, an isomorphous substitution can be obtained when Ca^{2+} is replaced by Zn^{2+} into dentine HAp (Osorio *et al.* 2014). These

data correlate with an augmentation of bands at 430 cm^{-1} and 451 cm^{-1} (v_2 mode) (~1.3 fold), assigned to vibration of carbonate calcium phosphate in apatite lattice (Timlin *et al.* 2000) (Table 2) (Fig 3e). $FWHM_c$ decreased (improved crystallinity referred to carbonate) when both PA+oxipatite and PA+calcypatite were used, being the crystallinity more pronounced when Zn was present (Table 2). On the other hand, conditioning with EDTA reduced crystallinity regardless of the type of biomaterial that was used (Table 2). As a consequence, this apatite resulted less mature by default of this poor crystallinity.

Collagen crosslinking is affected by the tissue maturation as well as the degree of mineralization, providing information about the structure and molecular interactions of complexes biomolecules (Xu & Wang, 2011; Saito *et al.* 2006). Ratios concerning the crosslinking of collagen reflected a movement toward higher frequencies after treating the dentine surface with PA+oxipatite, at 21 time point (Table 2). This shift denoted a general rise at 1032 (pyridinium), and 1550 cm^{-1} (AGES-Pentosidine) at the dentine surface (Fig 3e). The Raman intensities which evoke the nature and secondary structure of collagen *i.e.,* CH_2 (1450 cm^{-1}) and Ratio Amide I/A-III, (Table 2) lightly increased at dentine treated with PA+oxipatite, after 21 d of storage time (Table 2). This increase indicate recovery (Xu & Wang, 2012), better organization, improved structural differences and collagen quality (Salehi *et al.* 2013). Calcium hydroxide, present in calcypatite, induces matrix formation and mineralization probably through the stimuli for liberation of bone morphogenetic proteins, cytokines, and some specific tissue grown factors (Li *et al.* 2015). The hydroxyl group is considered the most important component of $Ca(OH)_2$ as it provides an alkaline environment, which encourages repair and active calcification (Mohammadi & Dummer, 2011). The alkaline pH activates alkaline phosphatases that play an important role in hard-tissue formation (Estrela *et al.* 1995). Alkaline phosphatase is a hydrolytic enzyme that acts by means of the liberation of inorganic phosphate from the ester of phosphate. It can separate phosphoric esters, freeing phosphate ions, which then react with local calcium ions to form a precipitate calcium phosphate, in the organic matrix. This precipitate is the molecular unit of HAp, which is believed to be intimately related to the process of mineralization (Mohammadi & Dummer, 2011). Even more, the organic matrix is composed of acid proteins and proteoglycans containing phosphate and carboxylate groups. These substances may act as bonding agents between the

collagen network and the HAp crystals (Bakland & Andreasen, 2012). In the present work, proteoglycans only increased when PA+oxipatite was applied and assessed after 21 d of storage time (Table 2).

At intertubular dentine, calcypatite application provoked a SRa augmentation after 21 d of study, regardless of the type of conditioning. Nevertheless, the use of PA gave rise to a ~ 5.33 fold higher increment of roughness in comparison with the use of EDTA (Fig 2a). It is believed that the formation of specific mineral nodules at dentine might have favored amorphous-bulk mineral precipitation at extrafibrillar compartment, leading to an augmentation of the surface roughness (Zurick *et al.* 2013). This demonstrated the lower potential for effective dentine remineralization that was achieved when PA+calcypatite was applied.

Through this manuscript we have attempted to provide evidence to support our claims that chemical changes occurring after treating the dentine surface with two different cleaner-conditioners, before the application of two canal sealers at two time points are going to provide modifications at the dentine surface. These are, to the best of our knowledge, the only available results from Raman spectroscopy combined with morphological and tribological nano-characterization of dentine. The null hypothesis that no changes in chemical and tribological properties were produced at dentine by the tested sealer cements, must be rejected. Relative to complementary experimental techniques that ultimately illustrate the clinical reaction of dentine, Field-emission SEM (FESEM), dark-field TEM (DF-TEM), High Resolution TEM (HRTEM), Scanning Transmission Electron Microscopy (STEM) and micro-XRD (μ-XRD), and fuzzy c-means cluster analysis (FCA) should be incorporated into our methodology, for future strategies of research. Therefore, the lack of these techniques may be considered as a limitation of the present study. Applying advanced technologies, both biofunctionality and biocompatibility studies should be carried out by using starting crystals for the production of hydroxyapatite for therapeutic dental applications in regions of demineralized dentine at the intra-canal compartment. This approach also deserves future research.

Conclusion

Dentine treated with phosphoric acid and oxipatite (PA+oxipatite) attained the smoothest dentine surface and the widest fibrils width, both linked to a high level of dentine mineralization.

Dentine treated with PA+oxipatite attainedthe greatest relative presence of minerals and calcification, thus providing an increase of both stoichiometric HAp and amorphous-like apatite species. The narrowing of the spectral peak width of carbonate indicated an increase of crystallinity when phosphoric acid was used, providing long degradation times for the new formed minerals. ~~and it also reduced~~ Dentine crystallinity was reduced when EDTA was used as conditioner with both biomaterials. EDTA promoted the formation of a lower stoichiometric and crystalline HAp than phosphoric acid, favoring the active dentine remodeling and hindering maturity.

Acknowledgements

This work was supported by the Ministry of Economy and Competitiveness (MINECO) [Project MAT2014-52036-P] and European Regional Development Fund (FEDER).

Conflict of interest

The authors (both the corresponding and co-authors) have stated explicitly that there are no conflicts of interest in connection with this article.

References

Ager JW, Nalla RK, Breeden KL, Ritchie RO (2005) Deep-ultraviolet Raman spectroscopy study of the effect of aging on human cortical bone. *Journal of Biomedical Optics* **10**, 034012.

Almahdy A, Downey FC, Sauro S, Cook RJ, Sherriff M, Richards D, Watson TF, Banerjee A, Festy F (2012) Microbiochemical analysis of carious dentine using Raman and fluorescence spectroscopy. *Caries Research* **46**, 432–40.

Al-Sanabani JS, Madfa AA, Al-Sanabani FA (2013) Application of calcium phosphate materials in dentistry. *International Journal of Biomaterials* **2013**, 876132.

Bakland LK, Andreasen JO (2012) Will mineral trioxide aggregate replace calcium hydroxide in treating pulpal and periodontal healing complications subsequent to dental trauma? A review. *Dental Traumatology* **28**, 25–32.

Barrère F, Layrolle P, Van Blitterswijk CA, De Groot K (2001) Biomimetic coatings on titanium: a crystal growth study of octacalcium phosphate. *Journal of Materials Science: Materials in Medicine* **12**, 529–34.

Bertassoni LE, Habelitz S, Pugach M, Soares PC, Marshall SJ, Marshall GW (2010) Evaluation of surface structural and mechanical changes following remineralization of dentin. *Scanning* **32**, 312–9.

Bonifacio A, Beleites C, Vittur F et al. (2010) Chemical Imaging of Articular Cartilage Sections with Raman Mapping, Employing Uni- and Multi-Variate Methods for Data Analysis. *The Analyst* **135**, 3193-204.

Carvalho CN, Freire LG, Carvalho AP, Duarte MA, Bauer J, Gavini G (2016) Ions Release and pH of Calcium Hydroxide-, Chlorhexidine- and Bioactive Glass-Based Endodontic Medicaments. *Brazilian Dental Journal* **27**, 325–31.

Cheng PT, Pritzker KP (1983) Pyrophosphate, phosphate ion interaction: effects on calcium pyrophosphate and calcium hydroxyapatite crystal formation in aqueous solutions. *Journal of Rheumatology* **10**, 769–77.

Estrela, C., Sydney GB, Bammann LL, Felippe Júnior O (1995) Mechanism of action of calcium and hydroxyl ions of calcium hydroxide on tissue and bacteria. *Brazilian Dental Journal* **6**, 85–90.

Fulmer MT, Brown PW. Effects of Na2HPO4 and NaH2PO4 on hydroxyapatite formation. Journal of Biomedical Materials Research Part A 1993; 27:1095–102.

Gandolfi MG, Ciapetti G, Taddei P *et al*. (2010) Apatite formation on bioactive calcium-silicate cements for dentistry affects surface topography and human marrow stromal cells proliferation. *Dental Materials* **26**, 974–92.

Habelitz S, Balooch M, Marshall SJ, Balooch G, Marshall GW (2002) In situ atomic force microscopy of partially demineralized human dentin collagen fibrils. *Journal of Structural Biology* **138**, 227–36.

Hoppe A, Güldal NS, Boccaccini AR (2011) A review of the biological response to ionic dissolution products from bioactive glasses and glass-ceramics. *Biomaterials* **32**, 2757–74.

Jean A, Kerebel B, Kerebel LM, Legeros RZ, Hamel H (1988) Effects of various calcium phosphate biomaterials on reparative dentin bridge formation. *Journal of Endodontics* **14**, 83-7.

Kitikuson P, Srisuwan T (2016) Attachment Ability of Human Apical Papilla Cells to Root Dentin Surfaces Treated with Either 3Mix or Calcium Hydroxide. *Journal of Endodontics* **42**, 89–94.

Kunstar A, Leijten J, van Leuveren S *et al*. (2012) Recognizing different tissues in human fetal femur cartilage by label-free Raman microspectroscopy. *Journal of Biomedical Optics* **17**, 116012.

Lee ML, Li Y, Feng YP, Carter CW (2002) Study of frequency dependence modulus of bulk amorphous alloys around the glass transition by dynamic mechanical analysis. *Intermetallics* **10**, 1061–4.

Li Y, Chen X, Fok A, Rodriguez-Cabello JC, Aparicio C (2015) Biomimetic Mineralization of Recombinamer-Based Hydrogels toward Controlled Morphologies and High Mineral Density. *ACS Applied Materials Interfaces* **7**, 25784–92.

Li Y, Thula TT, Jee S *et al*. (2012) Biomimetic mineralisation of woven bone-like nanocomposites: role of collagen cross-links. *Biomacromolecules* **13**, 49–59.

Liu Y, Kim YK, Dai L *et al.* (2011) Hierarchical and non-hierarchical mineralisation of collagen. *Biomaterials* **32**, 1291–1300.

Matsunaga K (2008) First-principles study of substitutional magnesium and zinc in hydroxyapatite and octacalcium phosphate. *Journal of Chemical Physics* **128**, 245101.

Mohammadi Z, Dummer PMH (2011) Properties and applications of calcium hydroxide in endodontics and dental traumatology. *International Endodontic Journal* **44**, 697–730.

Osorio R, Osorio E, Cabello I, Toledano M (2014) Zinc induces apatite and scholzite formation during dentin remineralization. *Caries Research* **48**, 276–90.

Osorio R, Sauro S, Watson TF, Toledano M (2015) Polyaspartic acid enhances dentine remineralization bonded with a zinc-doped Portland-based resin cement. *International Endodontic Journal*. doi: 10.1111/iej.12518. [Epub ahead of print].

Saito M, Fujii K, Marumo K (2006) Degree of mineralization-related collagen crosslinking in the femoral neck cancellous bone in cases of hip fracture and controls. *Calcified Tissue International* **79**, 160–8.

Salehi H, Terrer E, Panayotov I *et al*. (2013) Functional mapping of human sound and carious enamel and dentin with Raman spectroscopy. *Journal of Biophotonics* **6**, 765–74.

Takatsuka T, Tanaka K, Iijima Y (2005) Inhibition of dentine demineralization by zinc oxide: in vitro and in situ studies. *Dental Materials* **21**, 1170–7.

Takeyasu K, Omote H, Nettikadan S, Tokumasu F, Iwamoto-Kihara A, Futai M (1996) Molecular imaging of Escherichia coli F0F1-ATPase in reconstituted membranes using atomic force microscopy. *FEBS Letters* **392**,110-3.

Termine JD, Belcourt AB, Miyamoto MS, Conn KM (1980) Properties of dissociatively extracted fetal tooth matrix proteins. II. Separation and purification of fetal bovine dentin phosphoprotein. *Journal of Biological Chemistry* **255**, 9769–72.

Thian ES, Konishi T, Kawanobe Y *et al*. (2013) Zinc-substituted hydroxyapatite: a biomaterial with enhanced bioactivity and antibacterial properties. *Journal of Materials Science: Materials in Medicine* **24**, 437–45.

Timlin JA, Carden A, Morris MD, Rajachar RM, Kohn DH (2000) Raman spectroscopic imaging markers for fatigue-related microdamage in bovine bone. *Annals of Chemistry* **72**, 2229–36.

Toledano M, Aguilera FS, Osorio E, Cabello I, Toledano-Osorio M, Osorio R (2015) Self-etching zinc-doped adhesives improve the potential of caries-affected dentin to be functionally remineralized. *Biointerphases* **10**, 031002.

Toledano M, Aguilera FS, Osorio E, Cabello I, Toledano-Osorio M, Osorio R (2016) Efficacy and micro-characterization of pathophysiological events on caries-affected dentin treated with glass-ionomer cements. *International Journal of Adhesion and Adhesives* **69**, 91–109.

Tramini P, Pélissier B, Valcarcel J, Bonnet B, Maury L (2000) A Raman spectroscopic investigation of dentin and enamel structures modified by lactic acid. *Caries Research* **34**, 233–40.

Wang L, Zhao Y, Mei L *et al*. (2017) Effect of application time of maleic acid on smear layer removal and mechanical properties of root canal dentin. *Acta Odontologica Scandinavica* **75**, 59–66.

Xu C, Wang Y (2011) Cross-linked demineralized dentin maintains its mechanical stability when challenged by bacterial collagenase. *Journal of Biomedical Materials Research Part B: Applied Biomaterials* **96**, 242–8.

Xu C, Wang Y (2012) Collagen cross linking increases its biodegradation resistance in wet dentin bonding. *Journal of Adhesive Dentistry* **14**, 11–8.

Xu Z, Neoh KG, Lin CC, Kishen A (2011) Biomimetic deposition of calcium phosphate minerals on the surface of partially demineralized dentine modified with phosphorylated chitosan. *Journal of Biomedical Materials Research Part B: Applied Biomaterials* **98**, 150–9.

Zhao Z, Espanol M, Guillem-Marti J, Kempf D, Diez-Escudero A, Ginebra MP (2016) Ion-doping as a strategy to modulate hydroxyapatite nanoparticle internalization. *Nanoscale* **8**, 1595–1607.

Zurick KM, Qin C, Bernards MT (2013) Mineralization induction effects of osteopontin, bone sialoprotein, and dentin phosphoprotein on a biomimetic collagen substrate. *Journal of Biomedicals Material Research Part A* **101**, 1571–81.

Table 1. Materials and chemicals used in this study

<table>
<tr><td colspan="4">Product details</td></tr>
<tr><td rowspan="4">Calcypatite</td><td rowspan="2">Calcium hydroxide $(CaOH)_2$</td><td colspan="2">Basic formulation per 100 gr</td></tr>
<tr><td>Content and quantity (g)</td><td>Percentage (%)</td></tr>
<tr><td>Calcium hydroxide 45.0 g
Carbowax 400 40.0 g
Titanium dioxide 7.0 g
Aerosil 1.0 g
Barium Sulphate 7.0 g</td><td>42.5</td></tr>
<tr><td>Hydroxyapatite modified particles</td><td>Component and percentage
Calcium 39.2 %
Phosphorus 18.3 %
Magnesium < 0.1 %
Sodium < 0.1 %
Silicon 0.001-0.03 %
Other minor components < 0.005 %

Molar relation Ca/P 1.66</td><td>57.5</td></tr>
<tr><td rowspan="4">Oxiapatite</td><td rowspan="2">Zinc oxide (ZnO)</td><td colspan="2">Basic formulation per 100 gr</td></tr>
<tr><td>Content and quantity (g)</td><td>Percentage (%)</td></tr>
<tr><td>Zinc oxide (ZnO) 39.61 g
Titanium dioxide 5.8 g
Carbowax 400 40.0 g
Aerosil 2.0 g
Barium sulphate 14.8 g</td><td>42.5</td></tr>
<tr><td>Hydroxyapatite modified particles</td><td>Component and percentage
Calcium 39.2 %
Phosphorus 18.3 %
Magnesium < 0.1 %
Sodium < 0.1 %
Silicon 0.001-0.03 %
Other minor components < 0.005 %

Molar relation Ca/P 1.66</td><td>57.5</td></tr>
<tr><td colspan="4">Phosphoric acid 37% (Braun Medical SA, Barcelona, Spain).</td></tr>
<tr><td colspan="4">EDTA 17% (Sigma Aldrich, St. Louis, MO, USA).</td></tr>
<tr><td rowspan="2">Simulated Body Fluid Solution (SBFS)
pH=7.45</td><td>Sigma Aldrich, St. Louis, MO, USA</td><td colspan="2">NaCl 8.035 g
$NaHCO_3$ 0.355 g
$K_2HPO_4 \cdot 3H_2O$ 0.231 g, $MgCl_2 \cdot 6H_2O$ 0.311 g
1.0 M – HCl 39 ml
Tris 6.118 g</td></tr>
<tr><td>Panreac Química SA, Barcelona, Spain</td><td colspan="2">KCl 0.225 g
$CaCl_2$ 0.292 g
Na_2SO_4 0.072 g
1.0 M – HCl 0–5 ml</td></tr>
</table>

Table 2. Raman intensities (in arbitrary units) of mineral and organic components in calcypatite and oxipatite-treated dentine surfaces.

			Untreated dentine		EDTA 2'		PA 15''		Calcypatite				Oxipatite			
									EDTA 2'		PA 15''		EDTA 2'		PA 15''	
			24h	21d	24h	21d	24h	21d	24h	21d	24h	21d	24h	21d	24h	21d
MINERAL COMPONENTS																
Relative Presence of Mineral	Phosphate [961 cm^{-1}]	Peak	63.75	--	46.07	--	29.45	--	54.11	38.27	35.55	33.85	45.83	36.91	37.18	45.64
		Area	1620.42	--	1170.09	--	748.71	--	1373.33	971.3	752.02	859.06	1163.74	937.17	944.01	1158.54
		RMC_P	14.89	--	13.88	--	17.74	--	17.07	23.05	21.16	26.45	19.42	21.58	22.67	16.36
	Carbonate [1070 cm^{-1}]	Peak	6.72	--	5.17	--	3.64	--	6.04	4.72	4.2	4.57	5.41	4.3	4.66	5.28
		Area	222.92	--	128.65	---	135.55	--	199.84	136.84	156.18	170.04	156.86	160.1	154.38	153.19
		RMC_C	1.57	19.39	1.56	19.37	2.19	19.39	1.91	2.84	2.50	3.57	2.29	2.29	2.84	1.89
Crystallinity (FWHM)	Carbonate $FWHM_C$		--	--	--	--	--	--	--	19.36	--	19.36	--	19.36	--	19.36
	Phosphate $FWHM_P$		19.39	--	19.37	--	19.39	--	19.36	--	16.12	--	19.36	--	19.36	--
v2[430-431 cm^{-1}]			21.40	--	9.79	--	8.20	--	11.09	9.64	8.40	8.32	10.30	9.79	9.99	10.55
v2[451 cm^{-1}]			16.43	--	5.63	--	5.34	--	7.08	6.63	5.56	5.53	6.70	7.03	7.01	7.48
v1[954 cm^{-1}]			37.41	--	44.07	--	21.97	--	32.28	25.37	12.79	22.03	35.65	24.98	25.23	29.48
v1[956 cm^{-1}]			50.98	--	46.05	--	24.90	--	37.91	29.33	15.19	25.49	40.05	28.90	29.29	34.24
v1[963 cm^{-1}]			63.18	--	35.01	--	28.10	--	53.46	36.62	33.25	32.73	40.07	35.11	35.16	44.12
ORGANIC COMPONENTS																
Normalization	Phenyl [1003 cm^{-1}]		4.28	--	3.32	--	1.66	--	3.17	1.66	1.68	1.28	2.36	1.71	1.64	2.79
Crosslinking	Pyridinium [1032 cm^{-1}]		4.86	--	3.66	--	2.34	--	2.75	1.86	0.5	0.4	2.19	1.99	1.18	3.70
	AGEs-Pentosidine [1550 cm^{-1}]		0.48	--	0.57	--	0.21	--	0.27	0.23	0.28	0.14	0.12	0.27	0.11	0.42
Nature and secondary structure of collagen	A-III [1246-1270 cm^{-1}]		6.44	--	4.92	--	6.2	--	4.77	4.20	4.06	4.50	4.58	4.34	4.52	4.78
	CH_2 [1450 cm^{-1}]		2.27	--	1.89	--	2.06	--	1.98	1.69	1.63	2.15	2.18	1.80	1.78	2.08
	A-I [1655-1667 cm^{-1}]		1.83	--	2.60	--	0.57	--	0.34	-0,03	1.36	0.79	0.06	-0.05	0.47	0.47
	Ratio A-I/A-III		0.28	--	0.53	--	0.09	--	0.07	-0.01	0.33	0.18	0.01	-0.01	0.10	0.10
	Ratio A-III/ AGEs-pentosidines		13.42	--	8.63	--	29.52	--	17.67	18.26	14.50	32.14	38.17	16.07	41.09	11.38
	Proteoglycans [1062 cm^{-1}]		9.02	--	6.96	--	4.16	--	5.46	4.28	2.77	3.39	5.63	3.95	3.89	5.12
	α-helices [1340 cm^{-1}]		4.2	--	2.77	--	2.36	--	1.94	3.1	3.05	3.73	1.62	2.59	1.56	2.25

PA: Phosphoric acid; EDTA: Ethylene-diamine-tetraacetic acid; RMC: Relative Mineral Concentration between mineral/Phenyl (1003 cm^{-1}); FWHM: Full-width half-maximum; A: amide; AGEs: advanced glycation end products. For the organics components the peaks values had been normalized to the intensity of the Amide II band near 1510 cm-1. For the mineral components the peaks values had been normalized to the intensity of the symmetric phosphate band near 961 cm^{-1}.

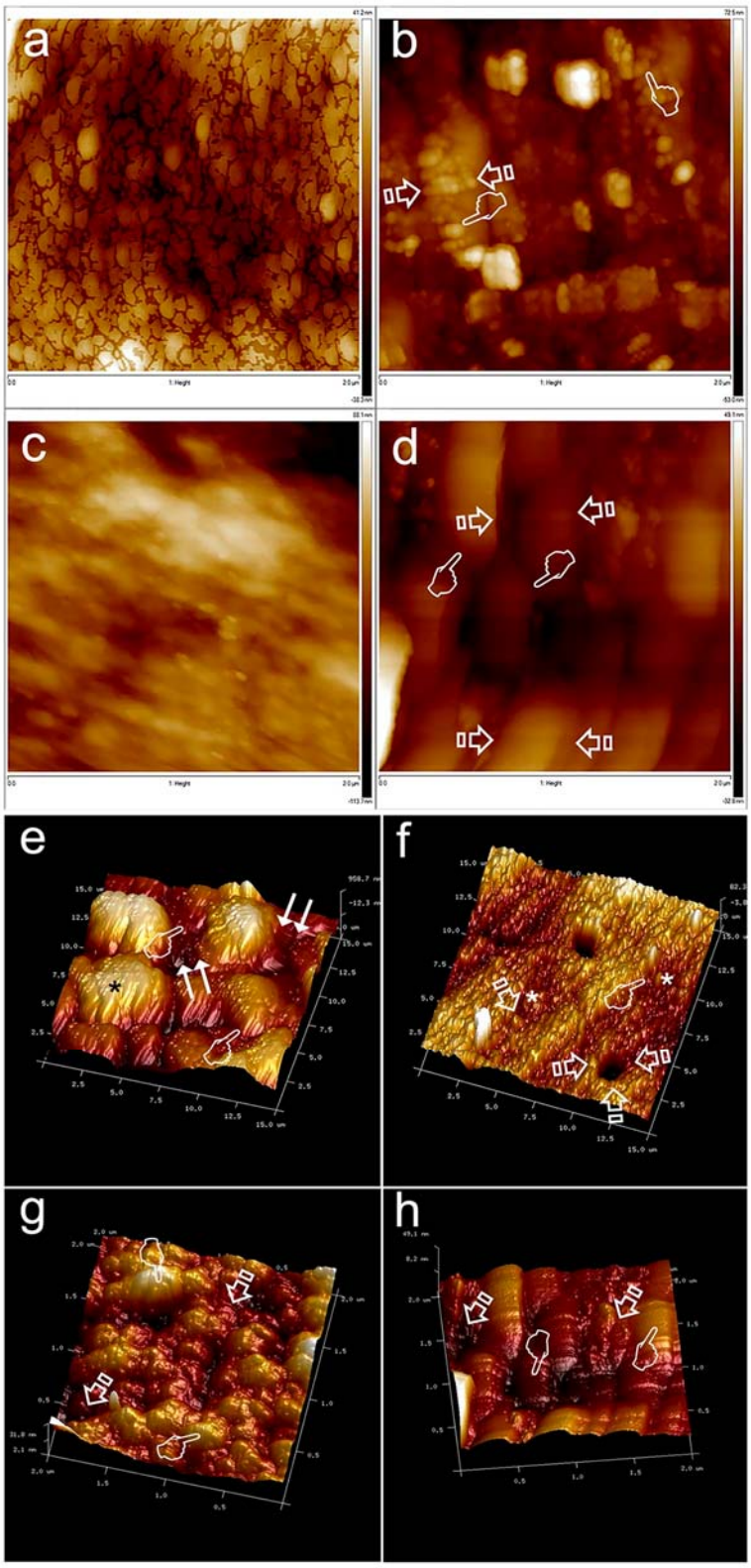

Figure 1. AFM phase image (2 x 2 µm) showing the bandwidth of the collagen fibrils in specimens treated with EDTA+calcypatite 24 h (**a**) or 21 d (**b**), PA+oxiapatite 24 h (**c**) or 21 d (**d**). Collagen fibrils, the bandwidth of these fibrils, and the wider bandwidth (faced arrows) with the staggered pattern of collagen fibrils are shown (pointers). AFM images of dentine treated with PA+calcypatite (**e**) and

PA+oxipatite (**f)**. At both figures a 15 x 15 μm surface plot image of the dentine surface is shown. Peritubular dentine is present (arrows) or absent (pointers). Extended mineral-depleted areas (double arrow) are reflected. Mineral tubular occlusion (asterisks) may be observed at the dentine surface. Some of these tubules figured completely occluded. Strong peritubular rings were formed at the entrance of some tubules (faced arrows) when zinc oxide was incorporated. AFM image (2 x 2 μm) of dentine surfaces treated with EDTA+oxipatite at 21 storage time (**g**). The dentine surface was showed medium-sized fibrils that appeared mineralized, with protruding rounded forms. The undulating topography corresponded with mineralized collagen (pointer), mineral deposits (arrows). AFM image (2 x 2 μm) of dentine surfaces treated with PA+oxipatite at 21 storage time (**h**). The dentine surface was covered by precipitated minerals (arrows). Underlying collagen fibers produced great prominence, resulting clearly visible (pointers).

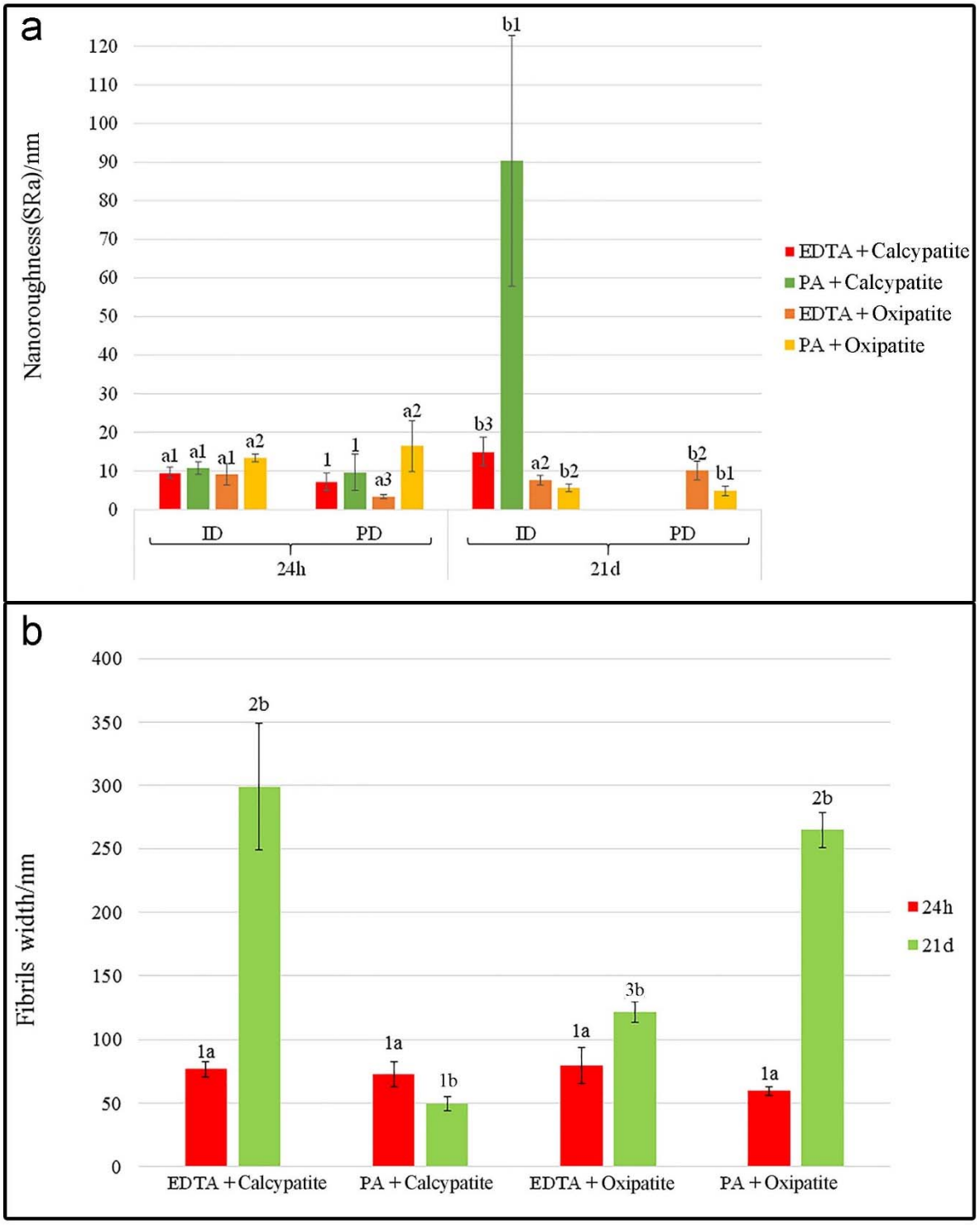

Figure 2. a, Mean and standard deviation of nanoroughness (SRa) (nm) at sound dentine surfaces of the different experimental groups. Same letter indicates no significant difference between 24 h and 21 d storage groups. Identical number indicates no significant differences between the different experimental dentine surfaces. SRa was not measured at peritubular dentine when calcypatite was used as it was not observable during the test. Abbreviations: EDTA, Ethylenediaminetetraacetic acid; PA, Phosphoric

acid; ID, Intertubular dentine; PD, Peritubular dentine. b, Mean and standard deviation of fibrils width (nm) at sound dentine surfaces of the different experimental groups. Same letter indicates no significant difference between 24 h and 21 d storage groups. Identical number indicates no significant differences between the different experimental dentine surfaces. Abbreviations: EDTA, Ethylenediaminetetraacetic acid; PA, Phosphoric acid.

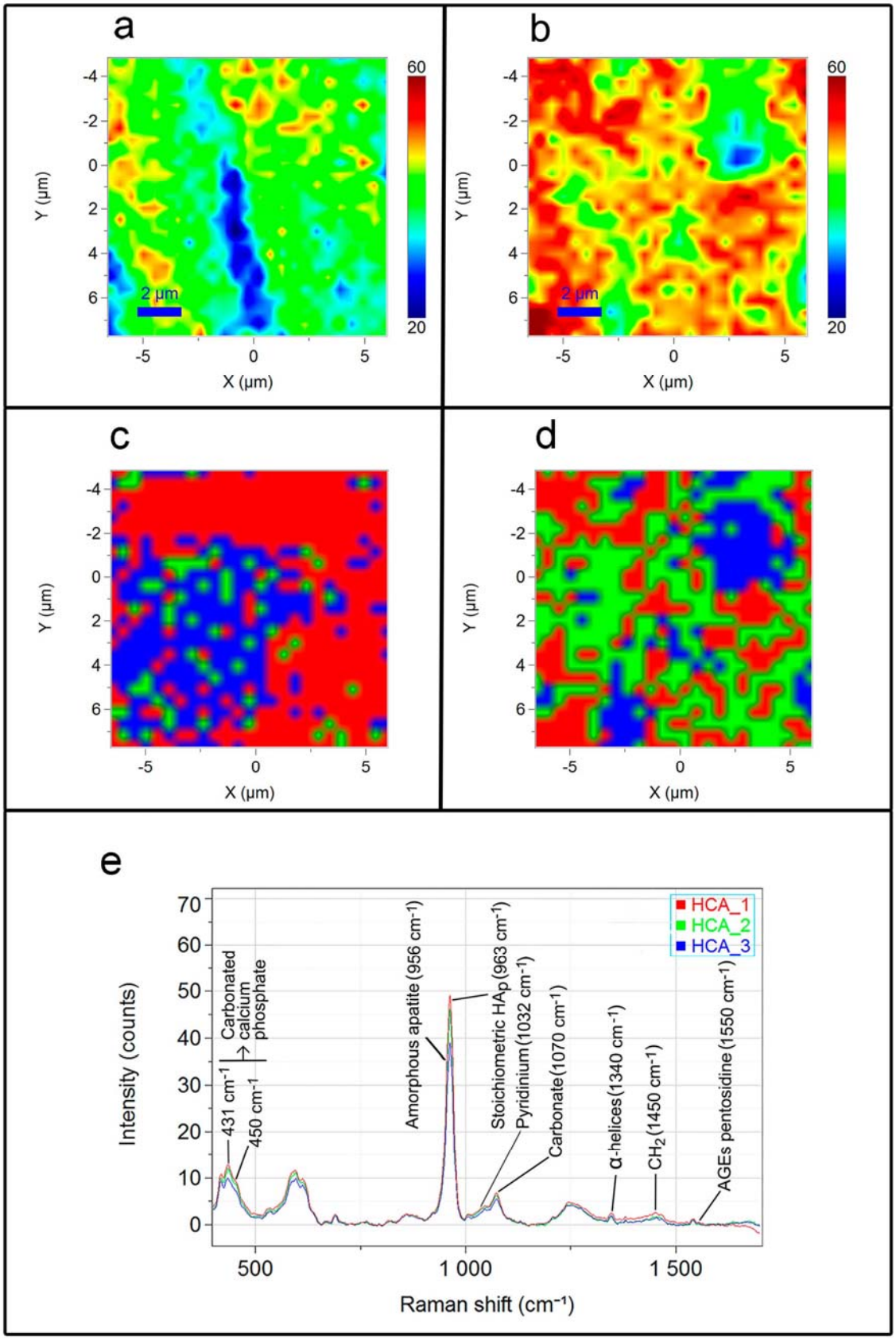

Figure 3. 2D micro-Raman map of the phosphate peak (961 cm-1) intensities at the groups PA+calcypatite (**a**) and PA+oxipatite (**b**), both at 21 d of storage time. Color mapping from hierarchical

cluster analysis **(**HCA) images corresponding to dentine surfaces treated with PA+calcypatite (**c**) and PA+oxipatite (**d**), both at 21 d of storage time. Three levels of HCA clustering are shown. Areas of distinct colors have differences in Raman spectral distribution and chemical composition. Each cluster, corresponding to a different dentine remineralization stage, is assigned to a different color (red, green, and blue), thus obtaining a false color-image of the substrate on the basis of similar spectral features. Spectra from hierarchical cluster analysis (HCA) results of dentine surfaces treated with PA+oxipatite, at 21 d of storage time (**e**).

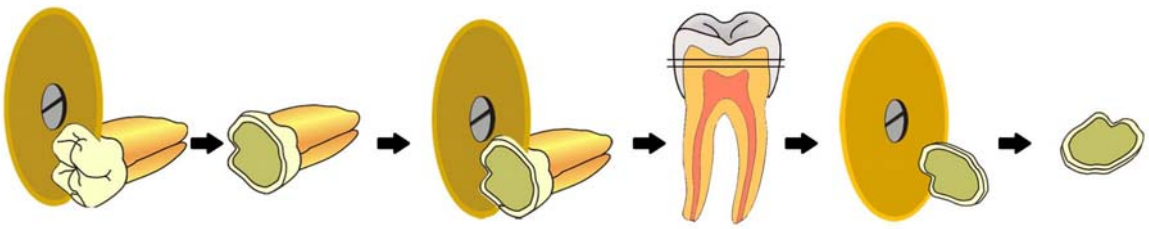

Supporting Information: Diagram 1. Graphical abstract illustrating the procedure to obtain the mid-coronal dentine disk.